

Minihalo photoevaporation during cosmic reionization: evaporation times and photon consumption rates

Ilian T. Iliev¹, Paul R. Shapiro,² and Alejandro C. Raga³

¹ *Canadian Institute for Theoretical Astrophysics, University of Toronto, 60 St. George Street, Toronto, ON M5S 3H8, Canada*

² *Department of Astronomy, University of Texas, Austin, TX 78712-1083*

³ *Instituto de Ciencias Nucleares, Universidad Nacional Autonoma de México (UNAM), Apdo. Postal 70-543, 04510 México, D. F., México*

12 November 2018

ABSTRACT

The weak, R-type ionization fronts (I-fronts) which swept across the intergalactic medium (IGM) during the reionization of the universe often found their paths blocked by cosmological minihaloes (haloes with virial temperatures $T_{\text{vir}} \leq 10^4$ K). When this happened, the neutral gas which filled each minihalo was photoevaporated; as the I-front burned its way through the halo, decelerating from R-type to D-type, all the halo gas was eventually blown back into the IGM as an ionized, supersonic wind. In a previous paper (Shapiro, Iliev & Raga 2004, hereafter Paper I), we described this process and presented our results of the first simulations of it by numerical gas dynamics with radiation transport in detail. For illustration we focused on the particular case of a $10^7 M_{\odot}$ minihalo which is overrun at $z = 9$ by an intergalactic I-front caused by a distant source of ionizing radiation, for different types of source spectra (either stellar from massive Pop. II or III stars, or QSO-like) and a flux level typical of that expected during reionization. In a Cold Dark Matter (CDM) universe, minihaloes formed in abundance before and during reionization and, thus, their photoevaporation is an important, possibly dominant, feature of reionization, which slowed it down and cost it many ionizing photons. In view of the importance of minihalo photoevaporation, both as a feedback mechanism on the minihaloes and as an effect on cosmic reionization, we have now performed a larger set of high-resolution simulations to determine and quantify the dependence of minihalo photoevaporation times and photon consumption rates on halo mass, redshift, ionizing flux level and spectrum. We use these results to derive simple expressions for the dependence of the evaporation time and photon consumption rate on these halo and external flux parameters which can be conveniently applied to estimate the effects of minihaloes on the global reionization process in both semi-analytical calculations and larger-scale, lower-resolution numerical simulations which cannot adequately resolve the minihaloes and their photoevaporation. We find that the average number of ionizing photons each minihalo atom absorbs during its photoevaporation is typically in the range 2–10. For the collapsed fraction in minihaloes expected during reionization, this can add ≈ 1 photon per total atom to the requirements for completing reionization, potentially doubling the minimum number of photons required to reionize the universe.

Key words: hydrodynamics—radiative transfer—galaxies: halos—galaxies: high-redshift—intergalactic medium—cosmology: theory

1 INTRODUCTION

The Cold Dark Matter model, due to its hierarchical nature, predicts that a significant fraction of the matter in the

arXiv:astro-ph/0408408v1 23 Aug 2004

universe before and during reionization (up to $\sim 30 - 40\%$ at redshift $z = 6$ for current Λ CDM) resided in collapsed and virialized minihaloes - small haloes with virial temperatures T_{vir} below 10^4 K. These minihaloes, in the mass range between the Jeans mass (below which gas pressure forces prevented baryonic matter in the IGM from collapsing into dark matter haloes as they formed; i.e. $M_J \lesssim 10^4 M_\odot$) and the mass for which $T_{\text{vir}} = 10^4$ K [$M(10^4 \text{ K}) \lesssim 10^8 M_\odot$] were filled with neutral gas, since their temperatures were too low for collisional ionization to be effective. Cosmic reionization had a profound effect on the gas content of these minihaloes and they, in turn, interfered with cosmic reionization.

This reionization began when the first sources of ionizing radiation turned on, causing global I-fronts to sweep outward through the surrounding IGM, creating intergalactic H II regions, and ended when these H II regions became large enough and numerous enough to overlap (Shapiro & Giroux 1987). These global I-fronts were generally weak, R-type fronts, which moved supersonically, not only with respect to the cold, neutral gas ahead of them but also with respect to the gas photoheated to $T \gtrsim 10^4$ K behind them. As such, they raced ahead of the hydrodynamical response of the ionized gas, unaffected by the disturbance they created in the gas behind them. That situation changed, however, when the path of one of these global I-fronts was blocked by a minihalo. Since the speed of an I-front varies inversely with the density of the neutral gas ahead of it, the I-front must have slowed down when it encountered the dense, centrally-concentrated gas inside a minihalo. The latter is, on average, more than a hundred times denser than the mean IGM, while at its center it is yet another hundred times denser even than that. This denser gas slowed the I-front down enough to “trap” it, long enough for the gas-dynamical back-reaction of the disturbed minihalo gas to catch-up to the I-front and affect its progress. Thereafter, the fate of this I-front and that of the minihalo gas were inextricably coupled, as ionized minihalo gas, heated to $T \geq 10^4$ K, above the binding energy of minihalo gravity, blew back toward the ionizing source, into the IGM as a supersonic, evaporative wind.

The first realistic discussion of the photoevaporation of cosmological minihaloes by global I-fronts during reionization, including the first radiation-hydrodynamical simulations of this process, was by Shapiro, Raga & Mellema (1997, 1998), developed further in Shapiro & Raga (2000a,b, 2001); Shapiro (2001) and Paper I (see Paper I for a more complete description and additional references.) As described in Paper I, the dominant sources of reionizing radiation are likely to have been haloes of virial temperature $T_{\text{vir}} \geq 10^4$ K. Star formation in minihaloes, instead, is thought to have been inhibited early on by the photodissociating effect on minihalo H_2 molecules of the rising UV background just below the H Lyman continuum edge, created by a small fraction of the sources ultimately required to complete reionization. If so, then each source of reionization would typically have found its sky covered by minihaloes between it and the nearest neighboring source haloes, and the expansion of I-fronts in the

IGM around each source to the point of overlap would have depended upon the photoevaporation of intervening minihaloes (Haiman, Abel & Madau 2001; Shapiro 2001; Barkana & Loeb 2002; Shapiro, Iliev, Raga & Martel 2003; Paper I). Since the gas inside collapsed minihaloes was much denser than average, the rate of recombination there was much higher than average, as well. Hence, minihalo photoevaporation was likely to have consumed multiple ionizing photons per atom, thereby increasing, and potentially dominating, the global photon consumption during reionization (Haiman, Abel & Madau 2001; Shapiro 2001; Paper I). Therefore, quantifying this process is crucial for determining the onset, progress and duration of the reionization of the universe.

An early start ($z \gtrsim 15$) and late finish ($z \approx 6$) for cosmic reionization are suggested by recent observations of the fluctuating polarization of the CMB (Kogut et al. 2003) and the Gunn-Peterson effect in the spectra of quasars at $z \approx 6$ (Becker et al. 2001, Fan et al. 2003), respectively. This is consistent with the view that the volume-filling factor of ionized regions of the universe grew over time from $z \gtrsim 15$ until they overlapped finally at $z \approx 6$. The presence of minihaloes filled with neutral gas was affected by this reionization, not only because photoevaporation stripped pre-existing minihaloes of their baryons, but also because the subsequent collapse of baryons into newly forming minihaloes was suppressed by “Jeans-mass filtering” of the linear density fluctuations in the baryonic component after the IGM was heated to $T \gtrsim 10^4$ K when it was reionized (Shapiro, Giroux, and Babul 1994; Shapiro 1995; Gnedin 2000b). These two processes acted to reduce the presence of neutral-gas-filled minihaloes only in the ionized regions, however. The neutral volume outside these regions continued to form new minihaloes without interruption, at the unfiltered rate of the universe without reionization. As a result, the I-fronts which led the expansion of the ionized regions would have advanced into neutral gas in which minihaloes formed with ever-increasing abundance over time. The unfiltered collapsed fraction in minihaloes for Λ CDM at $z = 20, 15, 9,$ and 6 was $3, 10, 28,$ and 36 percent, respectively (Paper I). The question of whether minihalo photoevaporation was a dominant feature of reionization will ultimately be answered only when we know the full story of cosmic reionization, since there also exist (somewhat more speculative) scenarios in which the formation of some minihaloes might have been suppressed by, for example, a significant X-ray background at high- z (e.g. Machacek, Bryan & Abel 2003, Glover & Brand 2003, Madau et al. 2004, Ricotti & Ostriker 2004), double reionization (Cen 2003), entropy floor (Oh & Haiman 2003), or reduced small-scale power in the power spectrum of primordial density fluctuations (Somerville, Bullock, & Livio 2003).

In Paper I, we discussed the process of photoevaporation of cosmological minihaloes in detail. We demonstrated the phenomenon of I-front trapping, whereby the highly supersonic, weak, R-type front propagating in the low-density IGM slows down upon entering the minihalo, where the gas density is much higher than that of the IGM, and converts to

D-critical and then subcritical D-type, preceded by a shock which compresses the gas ahead of the I-front. The I-front slowly propagates subsonically through the halo, stripping it of gas, layer by layer, as this gas, once ionized, expands into the IGM as a supersonic wind towards the ionizing source. This process eventually results in a dark matter halo completely devoid of gas. We described there in detail the structure and evolution of the photoevaporative flows and their dependence on the radiation spectrum of the external ionizing source, considering both massive stars (Pop II and Pop III) and QSO-like spectra. We derived the evolution of the position and speed of the I-front, the evolution of the halo's remaining neutral mass fraction and effective opaque geometric cross-section for the absorption of ionizing photons, as well as the global parameters of photoevaporation like the photoevaporation time, t_{ev} , and the number of ionizing photons absorbed per atom in the course of that evaporation, ξ , and its evolution. Finally, we also discussed some observational diagnostics of the photoevaporation process.

In this paper, we extend the results of Paper I by investigating the dependence of the photoevaporation process on the mass of the halo, on the level and spectrum of the external photoionizing flux responsible for the I-front which overtakes the halo, and on the redshift at which this I-front encounters the minihalo. As discussed in Paper I, we make the assumption that the H_2 molecule formation and cooling which might have led to star formation inside minihaloes were inefficient in the bulk of the minihalo population, so the minihaloes were largely “sterile” reservoirs of neutral atomic gas. We concentrate particularly on the dependence of the two properties of minihalo photoevaporation which are most important for quantifying their global effect on cosmic reionization, namely, the evaporation time t_{ev} and the net ionizing photon consumption rate per minihalo (i.e. the number of ionizing photons absorbed per minihalo atom during the evaporation time), ξ . In § 2, we shall define the quantities t_{ev} and ξ and how we use our simulations to evaluate them more precisely, and recall some approximations which have been used previously to estimate these quantities, for comparison. Our numerical simulations are described briefly in § 3. In § 4.1 and § 4.2, we summarize our numerical results for t_{ev} and ξ , respectively, for haloes of different masses encountered at different redshifts by the I-fronts driven by external ionizing sources of different flux levels and spectra, and compare these with the previous estimates described in § 2. In § 4.3, we show that the time-dependence of the evolving neutral mass fraction inside a minihalo during its evaporation has a universal shape, independent of halo parameters and external flux level. The implications of these results for the theory of cosmic reionization are briefly discussed in § 5. Throughout this paper we use the current concordance model for the background universe and the dark matter - flat, COBE-normalized ΛCDM with $\Omega_0 = 1 - \lambda_0 = 0.3$, $h = 0.7$ and $\Omega_b h^2 = 0.02$, with primordial density fluctuation power spectrum $P(k) \propto k^{n_p}$, with $n_p = 1$, and $\sigma_{8h^{-1}} = 0.87$ (e.g. Spergel et al. 2003).

2 HALO EVAPORATION TIMES AND IONIZING PHOTON CONSUMPTION RATES

We define the evaporation time t_{ev} to be the time at which only 0.1 per cent of the gas which was initially inside the minihalo remains neutral¹. As in Paper I, we then obtain the number of ionizing photons absorbed per minihalo atom during this evaporation time by directly counting the number of recombinations experienced by each of those initial halo atoms and its first ionization:

$$\xi(t) = \frac{N_{\text{ion}}}{N_a} + \frac{1}{N_a} \int_0^t dt \int dV (\alpha_{\text{H}}^{(2)} n_{\text{HII}} + \alpha_{\text{He}}^{(2)} n_{\text{HeII}}) n_e, \quad (1)$$

where n_e is the number density of electrons, n_{HII} and n_{HeII} are the number densities of H II and He II, respectively, while $\alpha_{\text{H}}^{(2)}$ and $\alpha_{\text{He}}^{(2)}$ are the Case B recombination coefficients for H II and He II, respectively, N_a is the total number of atoms initially inside the minihalo, and N_{ion} is the number of these atoms initially inside the minihalo which are ionized by the evaporation process. At time $t = t_{\text{ev}}$, practically all atoms originally in the minihalo are ionized, thus $N_{\text{ion}} = N_a$ and $\xi = \xi(t_{\text{ev}})$ is the total number of ionized photons consumed per minihalo atom. We have neglected the recombinations of He III to He II because these generally contribute diffuse flux which is absorbed on the spot by H and He.

Haiman, Abel & Madau (2001) estimated the evaporation times and photon consumption rates for evaporating minihaloes analytically as follows. The evaporation time t_{ev} was approximated by the sound-crossing time for the characteristic size of the minihalo at the sound speed of the ionized gas, $t_{\text{sc}} = 2r_t/c_s(10^4\text{K})$, roughly consistent with our earlier results for the simulation of the photoevaporation of a $10^7 M_{\odot}$ minihalo (Shapiro, Raga & Mellema 1997, 1998; Shapiro & Raga 2000a,b, 2001; Shapiro 2001). Haloes were assumed to be dark-matter dominated, nonsingular isothermal spheres according to the Truncated Isothermal Sphere (TIS) model (Shapiro, Iliev & Raga 1999; Iliev & Shapiro 2001). For a minihalo of mass M at high redshift z , the TIS halo solution yields

$$t_{\text{sc}} = 98 \text{ Myr } (M_7)^{1/3} \left(\frac{\Omega_0 h^2}{0.15} \right)^{-1/3} (1+z)_{10}^{-1} T_4^{-1/2}, \quad (2)$$

using the adiabatic sound speed $c_s(T) = 11.7(T_4/\mu)^{1/2} = 15.2 T_4^{1/2} \text{ km s}^{-1}$, where $\mu = 0.59$ is the mean molecular weight for fully ionized gas of H and He if the abundance of He is $A(\text{He}) = 0.08$ by number relative to H. Based on this evaporation time estimate, a naïve estimate of ξ is then made possible by further assuming that the minihalo has zero optical depth to ionizing photons and is fully ionized instantaneously but remains static at its initial density for a time t_{sc} (the optically-thin, static approximation, hereafter

¹ As discussed in Paper I, the evaporation time is not sensitive to the precise value adopted for this remaining neutral fraction in the definition, as long as the latter is much less than unity.

referred to as “OTS”). Ignoring the contribution of He to recombinations, equation (1) then yields

$$\xi_{\text{OTS}} = 1 + f \frac{C_{\text{int}} \langle n_H \rangle \alpha_H^{(2)}}{1 + \delta_{\text{TIS}}} t_{\text{sc}} \quad (3)$$

(Haiman, Abel & Madau 2001) (where we have added the first term on the r.h.s. above to their equation to account explicitly for the fact that each atom must first be ionized once before it can recombine and be ionized again), where $\langle n_H \rangle$ is the mean H atom number density inside a halo, $C_{\text{int}} \equiv \langle n_H^2 \rangle / \langle n_H \rangle^2 = 444^2$ is the effective clumping factor for the TIS, and $1 + \delta_{\text{TIS}} = 130.6$ is the average overdensity of a TIS halo with respect to the cosmic mean background density. The quantity f is an “efficiency factor” introduced to take account of details neglected by the OTS assumptions. Together, equations (2) and (3) yield

$$\xi_{\text{OTS}} = 1 + 206 f T_4^{-3/4} M_7^{1/3} \left(\frac{\Omega_0 h^2}{0.15} \right)^{-1/3} (1+z)_{10}^2. \quad (4)$$

Here, we have defined $M_7 \equiv M/10^7 M_\odot$ and $(1+z)_{10} \equiv (1+z)/10$. Haiman, Abel & Madau (2001) calibrated the factor f against an optically-thin simulation of the expansion of a uniformly photoheated halo (i.e. no radiative transfer), obtaining $f \approx 1$. According to this OTS approximation, $\xi_{\text{OTS}} \gg 1$ for minihaloes during cosmic reionization, thus the presence of minihaloes during cosmic reionization would have dramatically increased the number of ionizing photons needed to complete reionization (Haiman, Abel & Madau 2001). According to equation (4), that is, each atom which had collapsed into a minihalo before reionization ended would have consumed many ionizing photons during its photoevaporation, a disproportionately large share of the ionizing photon background compared to that which would be available to ionize the uncollapsed atoms in the diffuse IGM.

As shown by the detailed simulations in Paper I, for haloes of mass $10^7 M_\odot$ exposed at $z = 9$ to the typical level of ionizing radiation expected during reionization, while the OTS approximation yields a reasonable, rough estimate of t_{ev} , it grossly overestimates ξ , by factors of 30-50, depending on the ionizing source spectrum. This more accurate determination of ξ in Paper I by numerical hydrodynamical simulations with radiative transfer nevertheless showed that minihalo photoevaporation could still have consumed enough photons to increase substantially the total number required per baryon to complete reionization. By contrast, earlier estimates of the requirements for reionization of the IGM had concluded that only about one photon per atom was required, but these estimates were based on calculations without sufficient resolution to account for the minihaloes (Gnedin 2000a; Miralda-Escude, Haehnelt & Rees 2000). It is therefore crucial to extend the accurate determination of ξ in Paper I to the full range of minihalo masses, ionizing flux levels and redshifts expected during reionization, in order to evaluate the global effect of minihaloes on the process of reionization.

3 THE CALCULATION

3.1 Numerical Method and Initial Conditions

We have performed a large number of simulations of the photoevaporation of individual minihaloes which occurs when a weak, R-type intergalactic I-front encounters a minihalo during cosmic reionization. Our simulation method and initial conditions were described in some detail in Paper I, so we only briefly summarize these here. Each halo is modelled as a nonsingular TIS (Iliev & Shapiro 2001), surrounded by self-similar cosmological infall according to the solution of Bertschinger (1985). We generalized this self-similar infall solution to apply also to a low-density Λ CDM background universe at high redshift (Iliev & Shapiro 2001). At high- z , the halo radius for the current background cosmology adopted here is $r_t = 0.754 M_7^{1/3} (1+z_{\text{coll}})_{10}^{-1}$ kpc, the total atomic number density at the center is $n_0 = 3.2(1+z_{\text{coll}})_{10}^3 \text{ cm}^{-3}$, and the halo virial temperature and velocity dispersion are $T_{\text{vir}} = 4000 M_7^{2/3} (1+z_{\text{coll}})_{10}$ K and $\sigma_V = 5.2 M_7^{1/3} (1+z_{\text{coll}})_{10}^{1/2} \text{ km s}^{-1}$, respectively. For haloes with $T_{\text{vir}} \lesssim 10^4 \text{ K}$ (minihaloes), the gas atoms are neutral. We consider haloes in the mass range between the Jeans mass of the uncollapsed IGM prior to reionization, $M_J = 5.7 \times 10^3 (\Omega_0 h^2 / 0.15)^{-1/2} \times (\Omega_b h^2 / 0.02)^{-3/5} [(1+z)_{10}]^{3/2} M_\odot$, and the mass for which $T_{\text{vir}} = 10^4 \text{ K}$ according to the TIS model, $M(10^4 \text{ K}) = 3.95 \times 10^7 (\Omega_0 h^2 / 0.15)^{-1/2} [(1+z)_{10}]^{-3/2}$.

Our simulations use the two-dimensional, axisymmetric Eulerian gas-dynamics code CORAL, with radiative-transfer, Adaptive Mesh Refinement (AMR), and the van Leer Flux-Vector Splitting Algorithm, which resolves shocks well and properly tracks I-fronts ranging from fast, supersonic R-type to sub-critical, subsonic D-type, as described in detail in Paper I (and references therein). All our simulations were set up as we described in detail in Paper I. We fixed the size of the computational box in all simulations presented here to be the same in units of the halo radius (with the long side ~ 10 times larger than the halo radius), $x_{\text{box}} \propto r_{\text{vir}} \propto M_{\text{halo}}^{1/3} (1+z_{\text{coll}})^{-1}$, so that the fully-refined grid resolution is equivalent in all cases. As in Paper I, we consider three different cases for the spectrum of the external source of ionizing radiation: (1) starlight with a 50,000K black-body spectrum (hereafter, referred to as “BB5e4”), representative of massive Population II stars; (2) starlight with a 100,000K black-body spectrum (hereafter, “BB1e5”), as expected for massive Population III stars; and (3) QSO-like, with a power-law spectrum with spectral index -1.8 (hereafter, “QSO”). As in Paper I, we express the unattenuated external flux of ionizing photons as a dimensionless quantity, F_0 , the flux in units of that from a source emitting $N_{\text{ph}} = 10^{56} \text{ s}^{-1}$ ionizing photons per second at a proper distance d of 1 Mpc, or equivalently, emitting 10^{52} s^{-1} at a distance of 10 Kpc, so $F_0 \equiv F / \{10^{56} \text{ s}^{-1} / [4\pi(1 \text{ Mpc})^2]\} = N_{\text{ph}} / d_{\text{Mpc}}^2$.

Table 1. Numerical convergence test for the evaporation time t_{ev} and photon consumption rate per atom ξ as functions of grid resolution for minihalo of initial mass $10^7 M_{\odot}$, exposed to initial flux of $F_0 = 1$, starting at $z = 9$.

spectrum	N_{cell}	$(\Delta x)_{\text{min}}[\text{pc}]$	$r_t/(\Delta x)_{\text{min}}$	t_{ev} [Myr]	ξ
BB5e4	128×256	27.0	23.4	465	6.41
BB5e4	256×512	13.5	56.7	300	5.73
BB5e4	512×1024	6.7	113	195	5.39
BB5e4	1024×2048	3.4	227	150	5.14
QSO	128×256	27.0	23.4	112	6.20
QSO	256×512	13.5	56.7	103	5.45
QSO	512×1024	6.7	113	100	5.20
QSO	1024×2048	3.4	227	97	4.95
BB1e5	128×256	27.0	23.4	215	5.16
BB1e5	256×512	13.5	56.7	178	4.03
BB1e5	512×1024	6.7	113	145	3.39
BB1e5	1024×2048	3.4	227	128	3.33

3.2 Numerical Resolution

To begin, we have studied the numerical convergence of our simulations with increasing spatial grid resolution, for the quantities t_{ev} and ξ , in order to establish the limits of robustness and reliability of our results. We have performed a series of four simulations, with fixed halo parameters and external flux level, with our fully-refined grid resolution $N_{\text{cells}} = N_r \times N_x$, in 2D, axisymmetric (r, x) -coordinates, increasing by factors of 2 from 128×256 up to 1024×2048 , for each of the three incident spectra. The results are shown in Table 1. We note that with increasing resolution both the evaporation time t_{ev} and the number ξ of ionizing photons consumed per atom decrease, leading ultimately to convergence in both quantities at our highest resolution. The convergence is more readily achieved for the cases with harder spectra (QSO and BB1e5) than for the softer spectrum case BB5e4. In all cases ξ converges faster than t_{ev} .

3.3 Parameter space

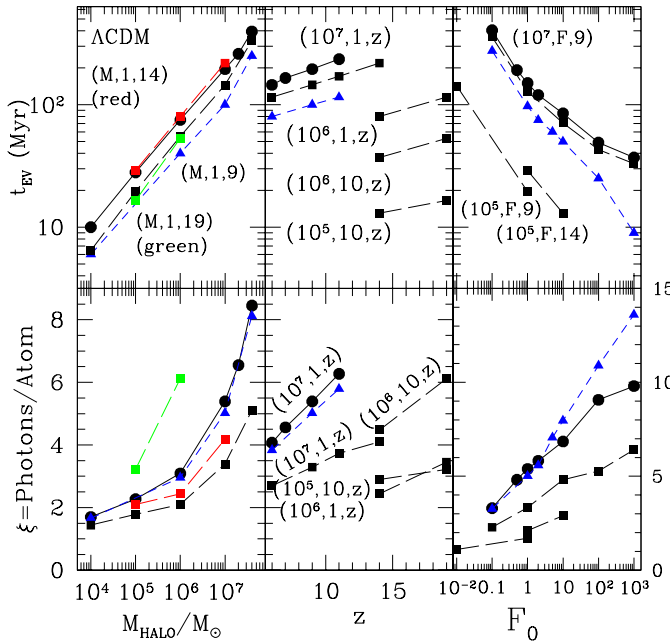
In order to study how the photoevaporation of minihaloes by global I-fronts during reionization depends upon the halo mass, the external ionizing flux level and spectrum, and the redshift at which the I-front encounters the minihalo, we have performed the following large set of simulations. We considered a range of halo masses from a low of $10^4 M_{\odot}$, which is close to the Jeans mass at the corresponding epoch, to $4 \times 10^7 M_{\odot}$, close to $M(10^4 K)$, the mass at which the halo virial temperature is $T_{\text{vir}} \sim 10^4 K$ (e.g. $M(10^4 K) = 4 \times 10^7 M_{\odot}$ at $z=9$). The intergalactic I-front which encountered the minihalo in each case was assumed to reach the boundary of our simulation volume at a starting redshift z_i (and we assumed $z_{\text{coll}} = z_i$ in defining the initial parameters of the TIS model for the halo). We took z_i to range from $1 + z_i = 20$, consistent with the early start for reionization implied by the recent WMAP results, to $1 + z_i = 7$, at which epoch the data from QSO absorption line spectra suggest that reionization was just ending. The flux levels assumed ranged from $F_0 = 0.01$ to $F_0 = 10^3$.

We argued in Paper I that the interval $F_0 = 0.01 - 100$ corresponds approximately to the typical range of fluxes expected when a global I-front encountered minihaloes during the reionization epoch. Here we extend this range up to $F_0 = 10^3$, to accommodate cases of very high flux due either to a rare, very strong source or to the minihalo's proximity to the source. In all our simulations the ratio of box size to halo radius was kept fixed at $L_{\text{box}}/r_t \sim 10$, which proved sufficient to follow the evaporation flow until full evaporation was achieved. Such a box size guaranteed that our transmissive boundary conditions were self-consistent at all times, since the simulation volume (fixed over time in proper coordinates) was always large enough to contain the sphere of radius equal to the turn-around radius in the cosmological infall profile centered on the minihalo as that radius increased over time. We show the complete set of simulation parameters and results for t_{ev} and ξ in Figure 1. In order to make such a large set of simulations feasible in terms of both computing time and storage requirements, we limited the degree of refinement of the mesh so that the fully-refined mesh had 512×1024 cells in all cases. Our numerical convergence tests above showed that, at this resolution, the simulations are already largely converged. To correct for any remaining small differences from the fully-resolved limit, we used the highest-resolution simulations in Table 1 to re-normalize our plotted results for t_{ev} ². Furthermore, in order to verify this approach, we performed a limited set of additional higher-resolution (1024×2048 fully refined) simulations for different halo masses and external fluxes as presented in Table 2.

² For BB5e4 and BB1e5 cases in Figure 1 which are not listed in Tables 1 and 2, the plotted points for t_{ev} are the actual values simulated at fully-refined grid resolution 512×1024 , adjusted slightly to correspond to the converged limit of our results for the highest grid resolution of 1024×2048 , based upon the convergence test results in Table 1. The adjusted values are 0.77 (0.88) times the simulation values for resolution 512×1024 for cases BB5e4 (BB1e5), respectively.

Table 2. Evaporation times and ionizing photon consumption rates per atom for several simulations at highest grid resolution (1024×2048 fully refined), all for $z_i = 9$ and $r_t/(\Delta x)_{\min} = 227$.

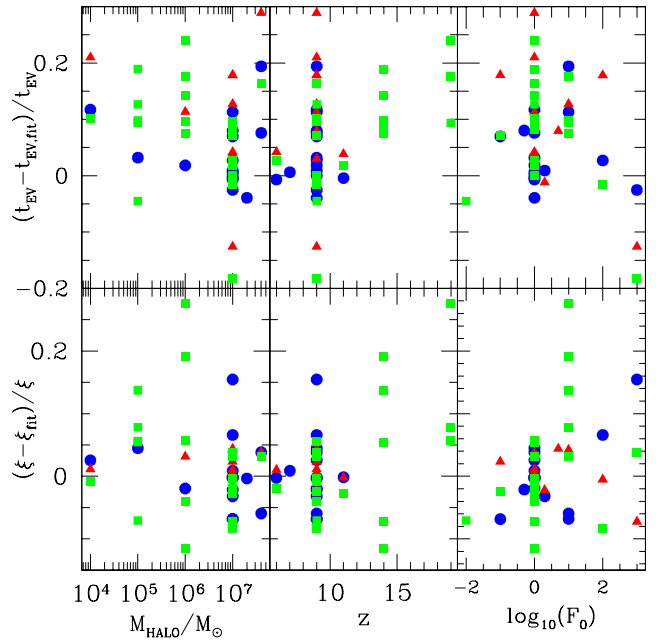
spectrum	F_0	M_7	$(\Delta x)_{\min}[\text{pc}]$	$t_{\text{ev}} [\text{Myr}]$	$t_{\text{ev}} [\text{Myr}] (\text{fit})$	ξ	$\xi (\text{fit})$
BB5e4	1	10^{-3}	0.34	8.5	7.5	1.75	1.71
BB5e4	10	4	5.4	170	137	10.6	11.2
BB5e4	0.5	1	3.4	210	193	4.7	4.8
BB5e4	10	1	3.4	85	75	6.85	7.3
BB5e4	10^2	1	3.4	49	47	9.07	8.5
BB5e4	10^3	1	3.4	37	38	9.80	8.3
QSO	10^2	1	3.4	25	21	10.9	11.0
QSO	10^3	1	3.4	9	10	13.6	14.6
BB1e5	10^2	1	3.4	41	41	5.28	5.7
BB1e5	10^3	1	3.4	29	34	6.41	6.2

**Figure 1.** Photoevaporation times t_{ev} for individual minihaloes (top panels) and total ionizing photon consumption per halo atom ξ (bottom panels) vs. halo mass M (left), redshift z at which I-front first encounters the minihalo (middle) and dimensionless ionizing flux F_0 (right), for the three different types of source spectra, BB5e4 (circles), QSO (triangles) and BB1e5 (squares), labelled by (M, F_0, z) to indicate the parameters which we kept fixed in each case as we varied the quantity on the x-axis. The red (green) lines on the two left panels correspond to redshift $1+z=15$ ($1+z=20$). Also, note the different vertical scale of the lower right panel only.

4 RESULTS

4.1 Evaporation time

Our simulation results for the evaporation time t_{ev} are plotted for all cases in Figure 1 (upper panels). The evaporation time increases significantly with increasing halo mass. For

**Figure 2.** Fractional errors of the fitting formulae in equations (5) and (6) compared with the simulation results for each of the cases plotted in Figure 1, for the evaporation times (top panels) and total ionizing photon consumption rates ξ (bottom panels), respectively, vs. halo mass M (left), redshift z at which I-front encounters the minihalo (middle) and dimensionless ionizing flux F_0 (right), for BB5e4 (blue circles), QSO (red triangles) and BB1e5 (green squares) spectra.

the smallest minihaloes $t_{\text{ev}} \sim 10$ Myr, much shorter than the Hubble time at that epoch, while for the larger minihaloes $t_{\text{ev}} \sim 100$ Myr, closer to, but still shorter than the current Hubble time. The redshift dependence of the evaporation time is even stronger than the mass dependence, with t_{ev} increasing with redshift. However, due to the relatively small range of the relevant redshifts, the overall variation of t_{ev} with redshift is only by factor of ~ 3 for fixed halo mass

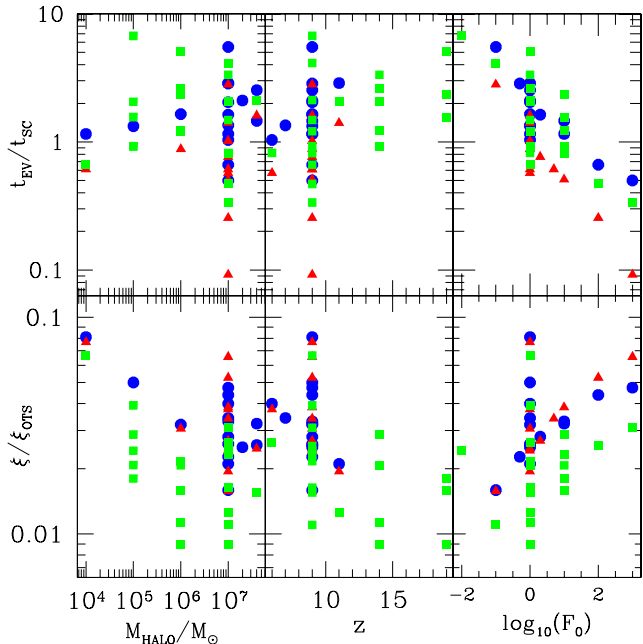


Figure 3. Comparison of simulation results for the evaporation times and photon consumption rates with predictions of the OTS approximation. Ratios of $t_{\text{ev}}/t_{\text{sc}}$ (top panels) and ξ/ξ_{OTS} (bottom panels) vs. halo mass M (left), redshift z at which I-front encounters the minihalo (middle) and dimensionless ionizing flux F_0 (right), for each of the cases plotted in Figure 1 for BB5e4 (blue circles), QSO (red triangles) and BB1e5 (green squares) spectra.

and external flux. Since the Hubble time $t_H \propto (1+z)^{-1.5}$, the evaporation times of higher-redshift haloes are a much larger fraction of the Hubble time, although still generally smaller than t_H . Finally, the evaporation times depend inversely on the level of the external ionizing flux, becoming extremely long ($t_{\text{ev}} \sim$ few hundreds of Myr) for low flux levels ($F_0 \lesssim 0.1$), and quite short ($t_{\text{ev}} \lesssim 30 - 40$ Myr) for high flux levels ($F_0 \gtrsim 10^2$).

The logarithmic slope of the dependence of t_{ev} on mass and the linear slope of its dependence on the initial redshift show no significant dependences on the source spectrum for the range of masses, fluxes and redshifts we have studied, although the overall normalization does vary. The dependence of t_{ev} on the flux is more complicated, with a slope which varies with F_0 .

A simple analytical fit to these results is given by

$$t_{\text{ev}} = AM_7^B F_0^{C+D \log_{10} F_0} \left[E + F \left(\frac{1+z}{10} \right) \right] \text{ Myr} \quad (5)$$

where $A = (150, 97, 128)$, $B = (0.434, 0.437, 0.465)$, $C = (-0.35, -0.357, -0.358)$, $D = (0.05, 0.01, 0.056)$, $E = (0.1, 0.3, 0.24)$, and $F = (0.9, 0.7, 0.76)$ for cases (BB5e4, QSO, BB1e5), respectively. We have fit the functional dependences based on all the points plotted in Figure 1. The relative errors of these fitting formulae are plotted in Fig-

ure 2 (upper panels) for all the cases in Figure 1. Table 2 shows the comparison between the simulation values and the fitting formulae for several of our highest-resolution simulations. In most cases the errors are $\lesssim 10\%$, and in all but two cases the errors are $\lesssim 20\%$.

We have compared our simulation results for t_{ev} with the OTS estimate of this quantity by Haiman, Abel & Madau (2001) in Figure 3. The OTS approximation, recall, assumes that the sound-crossing time of the halo once it is photoheated by ionizing radiation, $t_{\text{sc}} = 2r_t/c_s$, where c_s is the speed of sound at 10^4 K, is a good approximation to the evaporation time. According to equation (2), this means $t_{\text{ev,OTS}} = t_{\text{sc}} \propto r_t \propto M^{1/3}(1+z)^{-1}$, so the OTS evaporation time for a fixed halo mass *decreases* with increasing redshift in inverse proportion to the redshift, rather than *increasing* linearly with redshift, as in our numerical results, according to the scaling in equation (5), while the increase of t_{ev} with halo mass in the OTS prediction is somewhat less steep than our result. Finally, the OTS approximation completely ignores the significant dependence of t_{ev} on the magnitude and spectrum of the ionizing flux, making t_{sc} a significant underestimate of t_{ev} (by up to an order of magnitude) for low fluxes and a similarly significant overestimate for high fluxes.

4.2 Ionizing photon consumption

The simulation results for the number of ionizing photons per minihalo atom required to evaporate a minihalo, ξ , are plotted in Figure 1 (lower set of panels). The photon consumption per atom increases steeply with increasing halo mass. For the smallest minihaloes, $\xi \sim 2$, regardless of the spectrum of the ionizing source, i.e. each atom on average recombines just once during the evaporation of these haloes, or, equivalently, is ionized twice by the time it is expelled from the halo in the evaporative wind. On the other hand, for the larger minihaloes, the photon consumption rate is significantly larger, $\xi \sim 5 - 8$, so each atom in these haloes recombines multiple times on average during the evaporation of the halo. A BB1e5 source evaporates a large minihalo a factor of ~ 2 more efficiently in terms of photon consumption than a QSO or BB5e4 source, although the differences in efficiency between different spectra almost disappear for the smaller minihaloes. The ionizing photon consumption rate grows approximately linearly with redshift, and hence is noticeably higher at higher redshifts. Finally, opposite to the trend for the evaporation time, the photon consumption rate *grows* with increasing flux, with only 2-3 photons per atom needed in the case of low ionizing flux ($F_0 \lesssim 0.1$), but up to 7-16 needed in the case of high flux levels ($F_0 \gtrsim 10^2$). Therefore, and somewhat counter-intuitively, the low flux levels are much more efficient than the high flux levels, although the evaporation process takes much longer in the former than in the latter cases.

A good fit to these results is given by

$$\xi = 1 + AM_7^{B+C \log_{10} M_7} F_0^{D+E \log_{10} F_0} \left[F + G \left(\frac{1+z}{10} \right) \right], \quad (6)$$

where $A = (4.4, 4.0, 2.4)$, $B = (0.334, 0.364, 0.338)$, $C = (0.023, 0.033, 0.032)$, $D = (0.199, 0.24, 0.219)$, $E = (-0.042, -0.021, -0.036)$, $F = (0, 0, 0.1)$, $G = (1, 1, 0.9)$ for the BB5e4, QSO, and BB1e5 spectra, respectively. The relative errors of these scaling laws are plotted in Figure 2, lower panels. In most cases the errors are $\lesssim 10\%$, and in all cases but one the errors are below 20%.

We have compared our simulation results for ionizing photon consumption with the predictions of the OTS approximation in Figure 3. The OTS prediction for ξ is given by equation (4) with $f = 1$. The number of recombinations per atom, $\xi_{\text{OTS}} - 1$, scales with mass and redshift as $M^{1/3}(1+z)^2$. While the logarithmic slope of this OTS dependence on the halo mass is roughly similar to that of our simulations according to equation (6), the increase of ξ with redshift of the OTS prediction is much stronger than that of the simulation results. In addition, the dependence of ξ on the ionizing flux and spectrum is quite strong in the numerical results, while it is completely ignored in the OTS approximation. Unlike the evaporation time, t_{ev} , however, the overall normalization of ξ in the OTS approximation is overestimated by at least an order of magnitude in all cases, as compared with the simulation results, and by more than two orders of magnitude in some cases, particularly at high redshift and/or low ionizing flux levels.

4.3 Evolution of the neutral mass fraction

As described in Paper I, the first phase of the encounter between an intergalactic I-front and a minihalo is the weak, R-type phase, during which the I-front enters the halo and photoionizes an outer layer of halo gas, predominantly on the side facing the ionizing source, before the gas has time to respond hydrodynamically and move. This phase ends when the I-front slows to the R-critical speed and makes a transition to D-type, thereby trapping the I-front until it can burn through the remaining neutral, shielded minihalo gas and evaporate it. We identify the fraction of the original minihalo gas mass which was photoionized in this initial R-type phase when the front became R-critical as M_{cr} . We have plotted in Figure 4 the values of M_{cr} for our simulation cases in Figure 1. In Paper I, we derived an analytical approximation which can be used to estimate M_{cr} , called the Inverse Strömgen Layer (ISL) approximation, where ISL is the ionized boundary layer of the minihalo defined by the “outside-in” Strömgen length for each impact parameter (see Paper I for details). In the static, ionization-equilibrium approximation, the mass contained in this boundary layer, M_{ISL} , which is readily obtained for our TIS model by numerical integration as shown in Paper I, can be used to estimate M_{cr} as the complement of M_{ISL} , $M_{\text{cr}} = M_{\text{tot}} - M_{\text{ISL}}$.

In Paper I, we compared our simulation results for the ionized mass fraction at the transition from R-type to D-type for a $10^7 M_{\odot}$ halo exposed at $z_i = 9$ to a source of flux $F_0 = 1$ and found an excellent agreement with M_{ISL} . Here we extend the comparison to determine how well that agree-

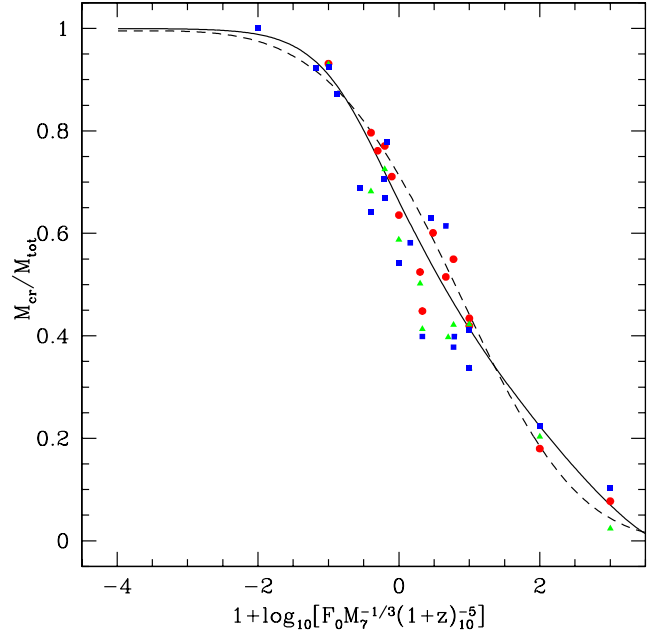


Figure 4. Neutral mass fraction of minihalo at the moment of I-front trapping, M_{cr} . Points show results from simulations with BB5e4 (circles), QSO (triangles) and BB1e5 (squares) spectra, respectively. For comparison, we plot the analytical prediction for this quantity derived from the Inverse Strömgen Sphere (ISL) approximation in Paper I (with argument on x-axis shifted as described in text), in which $M_{\text{cr,analyt}} \equiv 1 - M_{\text{ISL}}/M_{\text{tot}}$ (solid line), and a convenient fit to the ISL approximation and simulation results, according to equation (7) (dashed line).

ment holds up when we vary the halo parameters, source flux level, and redshift. We find that the dependence of the simulation results on these parameters follows that predicted by the ISL approximation fairly well, where the latter predicts that M_{ISL} should depend upon (M, F_0, z) only in the combination $F_0 M^{-1/3} (1+z)^{-5}$. We find, however, that the full range of simulation results for M_{cr} is better fit by this ISL scaling law if we multiply the quantity $F_0 M^{-1/3} (1+z)^{-5}$ in the original ISL approximation by 10. The excellent agreement between this modified ISL scaling law for M_{cr} and the simulation results is shown in Figure 4. We find that the following analytical expression provides a reasonable fit both to the ISL curve (with shifted argument) and the simulation results,

$$M_{\text{cr,approx}} = 0.9954 \exp(-0.0013x^4), \quad (7)$$

where $x \equiv 5 + \log_{10}[F_0 M_7^{-1/3} (1+z)_10^{-5}]$.

In Fig. 5 we show the evolution of the neutral mass fraction, M_n/M_{cr} vs. t/t_{ev} as the minihalo evaporates, for all of the cases plotted in Figure 1. This time-variation of the neutral mass fraction of the evaporating minihaloes is apparently a nearly universal function, when the neutral mass $M_n(t)$ is expressed in units of M_{cr} and t is expressed in units of t_{ev} for each case, independent of the halo parameters and

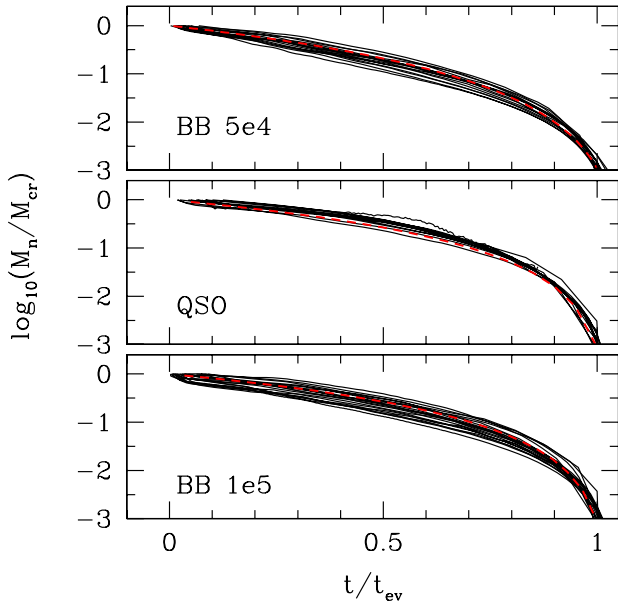


Figure 5. Evolution of the neutral mass fraction M_n/M_{cr} from the end of the initial R-type phase of the I-front and its conversion from R-type to D-type to the final evaporation of the halo, for simulations with BB5e4 (top), QSO (middle) and BB1e5 (bottom) spectra (solid lines). We also show the best fits in each case, as described in the text (long-dashed red lines).

external flux, but allows for some dependence on the spectrum of the external source. The scatter in all cases is largely due to the decrease of the flux level in time due to cosmological expansion, for a source located at fixed comoving distance from the target minihalo. Accordingly, the relation is tightest in the QSO case, since in these runs the evaporation times are shorter. The average shape of the neutral mass time-dependence function is well-fit by

$$M_n(t) = M_{cr} \left(1 - \frac{t}{At_{ev}}\right)^B, \quad (8)$$

where $A = (1.07, 1.03, 1.03)$ and $B = (2.5, 2, 2)$ for the BB5e4, QSO and BB1e5 spectra, respectively (red dashed lines in Fig. 5).

5 IMPLICATIONS FOR REIONIZATION AND CONCLUSIONS

The widespread presence of minihaloes filled with neutral gas during the epoch of reionization made encounters between the weak, R-type intergalactic I-fronts which ionized the IGM and these minihaloes a common occurrence. This interaction affected both the minihaloes and the I-fronts profoundly. The trapping of the I-fronts by minihaloes which cover the sky as seen by the more massive haloes which are generally believed to have been the primary sources of

cosmic reionization slowed the advance of those I-fronts in the IGM, at large, and wasted some of the ionizing radiation which would otherwise have been available to ionize that IGM. The minihaloes, in turn, were transformed by the photoevaporation which followed their trapping of the intergalactic I-fronts, into barren, dark-matter haloes devoid of baryons. In order to explore this process and its implications for cosmic reionization, we performed a large set of high resolution gas dynamical simulations which include radiative transfer, the first in their kind. In Paper I, we discussed our results in detail for the illustrative case of a $10^7 M_\odot$ halo which is overrun by an intergalactic I-front at $z_i = 9$, from a source of flux $F_0 = 1$, for different source spectra. Here we have summarized a much larger set of simulations designed to quantify the dependence of minihalo photoevaporation on the halo mass, source flux level and spectrum, and redshift. In Paper I, we discussed the comparison between our simulation results for $10^7 M_\odot$ haloes and previous related work. Here, we extend this comparison to include the broader set of cases presented in this paper.

We noted in Paper I that the approximate analysis of Barkana & Loeb (1999) which was used to argue that photoevaporation of minihaloes affected a significant part of the baryon fraction collapsed into haloes before the end of reionization was inconsistent with the results of our detailed numerical simulations for $10^7 M_\odot$ haloes. Barkana & Loeb (1999) had modelled this process by a static approximation like the ISL approximation in Paper I, to determine what portion of the halo’s mass is shielded from external ionizing photons and what portion is exposed to photoheating. They then assumed that only that portion which was instantaneously heated in this way, enough to unbind it from the halo gravitational potential well, would evaporate from the halo. From this static approximation, they concluded that only minihaloes smaller than $\sim \text{few} \times 10^5 - 10^6 M_\odot$ (depending on the redshift and the source spectrum) were evaporated completely during reionization, while the larger minihaloes would have retained a significant fraction of their gas (up to $\sim 50\%$ of the gas for haloes of mass $\approx \text{few} \times 10^7 M_\odot$). In Paper I we demonstrated that this model does not account properly for the dynamics of photoevaporation, and, as a result, it fails to anticipate the fact that even minihaloes as large in mass as $M = 10^7 M_\odot$ must ultimately evaporate completely. The larger set of simulations we have presented here show further that this neglect of dynamics by Barkana & Loeb (1999) in estimating the dependence of photoevaporation on halo mass is not correct; all minihaloes exposed to ionizing radiation during reionization evaporate completely. All of the gas initially in a minihalo would eventually have become unbound, outflowing with speeds of $v_{\text{wind}} = 20 - 40 \text{ km s}^{-1}$, leaving behind just a dark halo. The static approximation fails because it ignores the dynamical nature of photoevaporation. As evaporation proceeds, layers of gas are continuously stripped away, exposing the gas layers within to the ionizing radiation. Thus, although the inner halo region self-shields initially, all the gas is eventually “unshielded” and

photoheated to $T > 10^4$ K, well above the halo virial temperature, and, hence, boils out of the halo.

In Paper I we pointed out that simulations of the photoevaporation of $10^7 M_\odot$ haloes by an intergalactic I-front during reionization did not support the suggestion by Cen (2001) that external ionizing radiation can cause the implosion of the minihalo gas, leading to globular cluster formation. We did not observe such an effect in our simulations reported there. The broad range of cases considered here allow us to extend this comparison to the full range of parameter space expected for minihaloes exposed to the effects of externally-driven I-fronts during reionization. In no case have we yet found evidence of the implosion effect predicted by Cen (2001).

Our simulations show that the number of ionizing photons per minihalo atom needed to photoevaporate the minihalo is typically in the range $\xi \sim 2 - 10$, significantly larger than the value of $\xi \sim 1$ previously estimated to be sufficient to reionize the IGM (Gnedin 2000a; Miralda-Escude, Haehnelt & Rees 2000). On the other hand, we have also shown that recent claims (Haiman, Abel & Madau 2001) that the photoevaporation of minihaloes can require up to hundreds of ionizing photons per atom are very significantly overestimating ξ .

We have quantified here the dependence of evaporation times and photon consumption rates on the halo mass, source flux level and spectrum, and redshift of encounter between I-front and minihalo. We have provided convenient fitting formulae for our simulation results as functions of the parameters (M, F_0, z) , which should be useful in further analyses of the role of this process in cosmic reionization. To go beyond this step, it is necessary to determine the distribution in time and space of these parameters. The effect on reionization will depend upon the luminosity function of source haloes and the mass function of minihaloes as they evolve in time and fluctuate in space, including the clustering of both the sources and minihaloes. These may depend, in turn, upon the feedback of reionization on galaxy formation, so it is likely to be necessary to solve the problem of reionization in some detail before the true impact of minihaloes as screens and photon sinks is known. That is well beyond the scope of this paper. Here, instead, we shall provide a simple first estimate of the average effect of minihalo photon consumption on the photon budget required for reionization, based on the mean Press-Schechter (PS) distribution of minihaloes, as follows.

Let the ionizing photon consumption rate per minihalo atom be given for a single minihalo by $\xi(M, z, F_0)$. Then its average over all minihaloes at redshift z is given by

$$\bar{\xi}(z, F_0) = \frac{1}{\rho_{tot} f_{coll, MH}} \int_{M_{min}}^{M_{max}} \xi(M, z, F_0) M \frac{dn(M, z)}{dM} dM, \quad (9)$$

where $dn(M, z)/dM$ is the well-known PS mass function of haloes,

$$f_{coll, MH} \equiv \frac{1}{\rho_{tot}} \int_{M_{min}}^{M_{max}} M \frac{dn(M, z)}{dM} dM \quad (10)$$

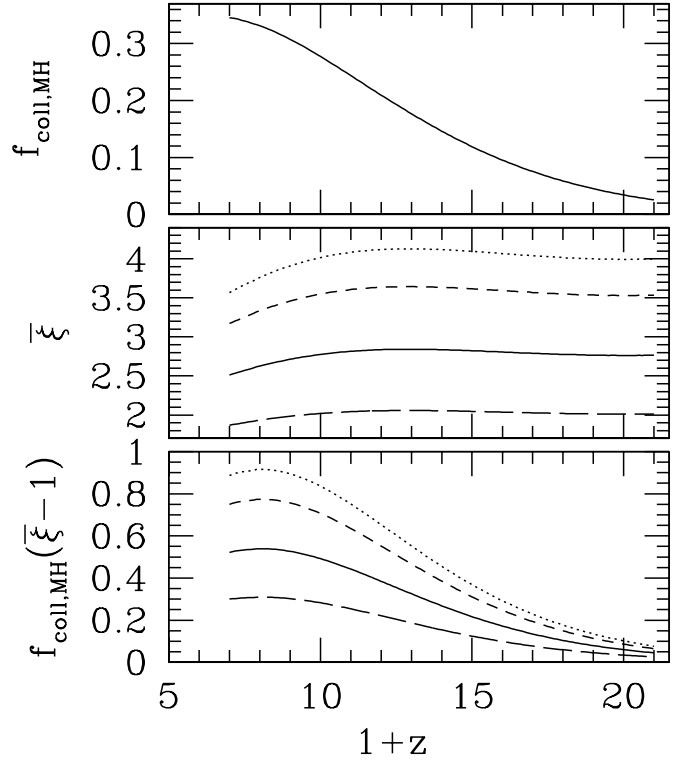


Figure 6. Collapsed fraction in minihaloes $f_{coll, MH}$ (top panel) for the Λ CDM universe, mean photon consumption per minihalo atom, $\bar{\xi}$, due to photoevaporation of minihaloes (middle panel), and mean excess photon consumption per total atom (i.e. all atoms, including both minihaloes and IGM) compared to the nominal requirement of one per atom (bottom panel). Results are for ionizing fluxes $F_0 = 0.1$ (long-dashed), 1 (solid), 10 (short-dashed) and 100 (dotted), for case BB5e4.

is the collapsed mass fraction in minihaloes, ρ_{tot} is the mean matter density at the corresponding redshift, M_{min} is the Jeans mass in the uncollapsed IGM, M_J , and $M_{max} = M(10^4 \text{K})$, is the halo mass corresponding to virial temperature 10^4 K. Assuming that $\xi(M, z, F_0)$ is given by the fitting formula in equation (6), we can calculate $\bar{\xi}(z, F_0)$ for any given redshift z and ionizing flux F_0 . Results for $F_0 = 0.1, 1, 10$ and 100 and $7 \leq 1+z \leq 21$ are shown in Figure 6, for case BB5e4. We see that $\bar{\xi}$ depends strongly on the ionizing flux ($\bar{\xi} \propto F_0^{0.199 - 0.042 \log_{10} F_0}$, in equation [6]), but is approximately independent of the redshift. Thus, the contribution of minihalo photoevaporation to the mean global photon consumption rate is largely dictated by the ionizing flux levels and the current collapsed fraction in minihaloes and can require up to ~ 1 additional ionizing photon per atom in the universe (both minihalo and IGM atoms) to finish reionization, as compared with the requirement when minihaloes are neglected, for the flux levels we considered

here. Hence, minihalo photoevaporation can potentially double the number of ionizing photons required to reionize the universe.

We defer the complete treatment of minihalo and source bias which would account for the spatially and temporally-varying fluxes during reionization to a future paper (Iliev, Scannapieco & Shapiro, in preparation). A brief summary of our first results along these lines can be found in Iliev, Scannapieco, Shapiro & Raga (2004), where it is shown that the statistical bias which causes the minihalo mass function to be enhanced around source haloes relative to the mean PS mass function boosts the relative contribution of minihaloes as photon sinks and compensates for the declining mean collapsed fraction at high redshift.

This shows that minihalo photoevaporation will be an important feature of reionization, causing a modest, but significant slow down of the global I-fronts and delaying their overlap. Only a more detailed, self-consistent treatment of the global process for a given reionization scenario will determine if reionization was photoevaporation-dominated, since the influence of minihaloes is strongly dependent on both the flux and, through the evolving collapsed fraction, the redshift at which the I-fronts encountered the minihaloes. Additionally, minihalo formation in some places and at some epochs might be partially suppressed by e.g. an early X-ray background, double reionization, or reduced small scale power. Such different scenarios might be distinguished observationally by detecting the fluctuations of the redshifted 21-cm emission or absorption lines from minihaloes (Iliev et al. 2002, 2003; Cen 2003) or the kind of absorption line signatures at UV and optical wavelengths discussed in Paper I.

ACKNOWLEDGMENTS

We thank Andrea Ferrara and Garrelt Mellema for many useful discussions. This research was supported by NSF grant INT-0003682 from the International Research Fellowship Program and the Office of Multidisciplinary Activities of the Directorate for Mathematical and Physical Sciences, the Research and Training Network "The Physics of the Intergalactic Medium" set up by the European Community under the contract HPRN-CT2000-00126 RG29185, NASA ATP grants NAG5-10825 and NNG04G177G and Texas Advanced Research Program grant 3658-0624-1999.

REFERENCES

- Barkana R., Loeb A. 1999, ApJ, 523, 54
 Barkana R., Loeb A. 2002, ApJ, 578, 1
 Bertschinger E., 1985, ApJS, 58, 39
 Cen R. 2001, ApJ, 560, L592
 Cen R. 2003, ApJ, 591, 12
 Glover S. C. O., Brand P. W. J. L. 2003, MNRAS, 340, 210
 Gnedin N. Y. 2000, ApJ, 535, 530
 Gnedin N. Y. 2000, ApJ, 542, 535
 Haiman Z., Abel T., Madau P., 2001, ApJ, 551, 599
 Iliev I. T., Shapiro P. R., Scannapieco E., Raga A. C. 2004, in *Outskirts of Galaxy Clusters: Intense Life in the Suburbs* (Proceedings of IAU Colloquium 195), ed. A. Diaferio, Cambridge University Press, in press
 Iliev I. T., Scannapieco E., Martel H., Shapiro P. R. 2003, MNRAS, 341, 81
 Iliev I. T., Shapiro P. R. 2001, MNRAS, 325, 468
 Iliev I. T., Shapiro P. R., Ferrara A., Martel H. 2002 ApJ, 572, L123
 Machacek M. E., Bryan G. L., Abel T. 2003, MNRAS, 338, 273
 Madau P., Rees M. J., Volonteri M., Haardt F., Oh S. P. 2004, ApJ, 604, 484
 Miralda-Escude J., Haehnelt M., Rees M. J., 2000, ApJ, 530, 1
 Oh S. P., Haiman Z. 2003, MNRAS, 346, 456
 Ricotti M., Ostriker J. P. 2004, MNRAS, 352, 547
 Shapiro P. R. 1995, in *The Physics of the Interstellar Medium and Intergalactic Medium*, A. Ferrara, C.F. McKee, C. Heiles, P.R. Shapiro eds., (ASP Conference Series, Volume 80), p.55
 Shapiro P. R. 2001, in *Relativistic Astrophysics: 20th Texas Symposium*, eds. J. C. Wheeler & H. Martel (AIP Conf. Proc. 586), pp. 219-232
 Shapiro P. R., Giroux M. L. 1987, ApJ, 321, L107
 Shapiro P. R., Giroux M. L., Babul, A. 1994, ApJ, 427, 25
 Shapiro P. R., Iliev I. T., Raga A. C. 1999, MNRAS, 307, 203
 Shapiro P. R., Iliev I. T., Raga A. C. 2004, MNRAS, 348, 753 (Paper I)
 Shapiro P. R., Iliev I. T., Raga A. C., Martel H. 2003 in *The Emergence of Cosmic Structure*, eds. Holt, S. S. & Reynolds, C. S. (AIP Conf. Proc. 666), pp. 89-92
 Shapiro P. R., Raga A. C. 2000, in *Astrophysical Plasmas: Codes, Models, and Observations*, eds. S. J. Arthur, N. Brickhouse, & J. J. Franco, *Rev.Mex.A.A. (SC)*, 9, 292
 Shapiro P. R., Raga A. C. 2000, in *Cosmic Evolution and Galaxy Formation: Structure, Interactions, and Feedback*, eds. J. Franco, E. Terlevich, O. Lopez-Cruz, & I. Aretxaga, (ASP Conference Series, vol. 215), pp. 1-6
 Shapiro P. R., Raga A. C. 2001, in *The Seventh Texas-Mexico Conference on Astrophysics: Flows, Blows, and Glows*, eds. W. Lee & S. Torres-Peimbert, *Rev.Mex.A.A. (SC)*, vol. 10, pp. 109-114
 Shapiro P. R., Raga A. C., Mellema G. 1997, in *Structure and Evolution of the Intergalactic Medium from QSO Absorption Line Systems* (Proceedings of the 13th IAP Astrophysics Colloquium), eds. P. Petitjean & S. Charlot, pp. 41 -45
 Shapiro P. R., Raga A. C., Mellema G. 1998, MmSAI, 69, 463
 Somerville R. S., Bullock J. S., Livio M. 2003, ApJ, 593, 616
 Spergel D. et al. 2003, ApJS, 148, 175